**Manuscript for submission to
Solid Earth**

**Shear wave reflection seismics yields subsurface
dissolution and subrosion patterns: application to the
Ghor Al-Haditha sinkhole site, Dead Sea, Jordan**

Ulrich Polom[1]*, Hussam Alrshdan[2], Djamil Al-Halbouni[3], Eoghan P. Holohan[4], Torsten Dahm[3,7], Ali Sawarieh[2], Mohamad Y. Atallah[5], and Charlotte M. Krawczyk[3,6]

1. Leibniz Institute for Applied Geophysics (LIAG), Stilleweg 2, D-30655 Hannover, Germany, ulrich.polom@liag-hannover.de

2. Ministry of Energy and Mineral Resources (MEMR), P.O.Box 7 code 11118, Amman, Jordan, hussam.rshdan@MEMR.GOV.JO, Ali.Sawarieh@MEMR.GOV.JO

3. GFZ German Research Centre for Geosciences, Telegrafenberg, D-14473 Potsdam, Germany, halbouni@gfz-potsdam.de, torsten.dahm@gfz-potsdam.de, lotte@gfz-potsdam.de

4. UCD School of Earth Sciences, University College Dublin, Dublin 4, Ireland, eoghan.holohan@ucd.ie

5. Yarmouk University 21173, Department of Geological and Environmental Science, Irbid, Jordan, matallah@yu.edu.jo

6. Technische Universität Berlin, Institute of Applied Geosciences, Ernst-Reuter-Platz 1, D-10587 Berlin, Germany, charlotte.krawczyk@tu-berlin.de

7. University of Potsdam, Institute of Earth and Environmental Sciences, D-14476 Potsdam, Germany

correspondence to: Ulrich Polom (Ulrich.Polom@liag-hannover.de)

Abstract.

Near-surface geophysical imaging of alluvial fan settings is a challenging task, but crucial for understating geological processes in such settings. The alluvial fan of Ghor Al-Haditha at the southeast shore of the Dead Sea is strongly affected by localized subsidence and destructive sinkhole collapses,

40   with a significantly increasing sinkhole formation rate since ca. 1983. A similar increase is observed also on the western shore of the Dead Sea, in correlation with an ongoing decline of the Dead Sea level. Since different structural models of the upper 50 m of the alluvial fan and varying hypothetical sinkhole processes have been suggested for the Ghor Al-Haditha area in the past, this study aimed to clarify the subsurface characteristics responsible for sinkhole development.

45   For this purpose, high-frequency shear wave reflection vibratory seismic surveys were carried out in the Ghor Al-Haditha area along several crossing and parallel profiles with a total length of 1.8 km and 2.1 km in 2013 and 2014, respectively. The sedimentary architecture of the alluvial fan at Ghor Al-Haditha is resolved down to a depth of nearly 200 m in high-resolution, and is calibrated with the stratigraphic profiles of two boreholes located inside the survey area.

50   The most surprising result of the survey is the absence of evidence for a thick (>2-10 m) compacted salt layer formerly suggested to lie at ca. 35-40 m depth. Instead, seismic reflection amplitudes and velocities image with good continuity a complex interlocking of alluvial fan deposits and lacustrine sediments of the Dead Sea between 0-200 m depth. Furthermore, the underground of areas affected by sinkholes is characterized by highly-scattering wave fields and reduced seismic interval velocities. We propose that

55   the Dead Sea mud layers, which comprise distributed inclusions or lenses of evaporitic chloride, sulphate, and carbonate minerals as well as clay silicates, become increasingly exposed to unsaturated water as the sea level declines, and are consequently destabilized and mobilized by both dissolution and physical erosion in the subsurface. This new interpretation of the underlying cause of sinkhole development is supported by surface observations in nearby channel systems. Overall this study shows that shear wave

60   seismic reflection technique is a promising method for enhanced near-surface imaging in such challenging alluvial fan settings.

Keywords

shallow reflection seismics, high-resolution, Vibroseis, sinkholes, Dead Sea, shear waves

1. Introduction

65

Since around 1980 until today, thousands of sinkholes have affected specific areas along the Dead Sea shoreline (Yechieli et al., 2006, Shalev et al., 2006, Abelson et al., 2017), apparently contemporaneous with the rapid decrease of the Dead Sea level (Sawarieh and Alrshdan, 2011). The sinkhole processes continuously disrupt farming areas, houses, industrial sites, and infrastructure, and, therefore, hamper the

70 future economic development of the whole region. Geological and geophysical sinkhole studies started already in the 1990's at both the western (e.g. Wachs et al., 2000) and eastern (El-Isa et al., 1995) shorelines of the Dead Sea. An early map of the main sinkhole sites was published by Yechieli et al. (2002). The sinkholes typically appear in clusters on either alluvial fans or mud flats. Arkin and Gilat (2000) defined two different classes of sinkholes: a) gravel holes on alluvial fans that consist of highly

75 permeable gravel and sand layers including some silt, clay and evaporites; and b) mud holes on Dead Sea mud flats that consist of very fine marl, silt, clay and evaporitic minerals like aragonite, gypsum and halite.

An early hypothesis postulated that clay softening, liquefaction and mobilization in the subsurface, due to the dilution of former highly salty porewater by freshwater inflows, generates the sinkholes (Arkin and

80 Gilat, 2000). As discussed by Ezersky and Frumkin (2013), two other factors may control the location of the sinkholes at the Dead Sea: (1) the presence of a thick, massive salt layer that is exposed to a dissolution front at its edge, and (2) the presence of sub-surface faults that control fresh water inflow into, and thus enable dissolution of, a salt layer. Such controls were suggested on the basis of a variety of methical approaches (e.g. Yechieli et al., 2002, Diabat, 2005, Closson, 2005, Abelson et al., 2006,

85 2009, Ezersky, 2006, Frydman et al., 2008, Closson and Abou Karaki, 2009, Ezersky et al., 2010, Ezersky, 2013c, Ezersky and Livne, 2013, Ezersky et al., 2017).

Although many geophysical studies have been carried out at the Ghor Al-Haditha sinkhole site (**Fig. 1a**) in the past 24 years, the subsurface structure and the subsurface erosion (subrosion) processes are still rather uncertain. Since the year 2000, several authors have proposed that a several metre thick, massive

90 salt layer lies at top depth of 35-40 m below the ground surface at the site, underneath the alluvial fan deposits (Taqieddin et al., 2000, Legchenko et al., 2008, Frumkin et al., 2011, Ezersky et al., 2013 a,b,c, Ezersky and Frumkin, 2013, Ezersky and Livne, 2013, Ezersky et al., 2017). In this shallow salt layer model, chemical erosion (dissolution) of this salt layer by fresh water flow from the eastern mountain range is supposed to generate initial cavities in the subsurface, which subsequently move upwards due to

95 continuous solution or collapse of material at the cavity top, up to the final collapse of the ground surface. In contrast, Al-Halbouni et al. (2017) presented an alternative conceptual model for Ghor Al-Haditha, based on photogrammetric surveying, historic satellite image analysis and field observations. They propose both chemical and physical subrosion of weak material, which consists both of mud flat (including evaporite lenses) and alluvial fan sediments.

100

Figure 1: (a) Generalized map of the Dead Sea area. Except the site Ghor Al-Haditha at the eastern border, which is the focus of this paper, the most sinkhole sites are located along the western shoreline of the Dead Sea (see e.g. Yechieli et al. 2002). (b) detailed map of the Ghor Al-Haditha sinkhole site and previous refraction seismic (El-Isa et al., 1995, Sawarieh et al., 2000) and MASW (Bodet et al., 2010) profiling. Boreholes BH1 and BH2 are reported in detail by El-Isa et al. (1995), two other boreholes are reported by Bodet et al. (2010) without any further information. Background is a Pleiades satellite image from 2015 combined with an aerial orthophoto mosaic from 2016.

Our reflection seismic study resolves for the first time the fine structure of subsurface layers with high-resolution at Ghor Al-Haditha, and thereby contributes to reappraising the different models suggested above. We further show that shear wave reflection seismics has advantages to study highly porous, partly saturated alluvial fans with complex compositions. A particular methodological question of interest is to what extent shear wave seismics can be used to identify dissolution processes at depth and early stages of collapse sinkholes.

2. Site of investigation

Ghor Al-Haditha is a small village at the south-eastern end of the Dead Sea in the province Al-Karak of the Hashemite Kingdom of Jordan (**Fig. 1 a&b**). It is located within the Dead Sea pull-apart basin close to the outlet of the Wadi Ibn Hammad valley. Sediments transported down the Wadi Ibn Hammad and the

neighbouring Wadi Mutayl have formed a connected alluvial sediment plain, which is in contact with the
120   border of the Dead Sea. The alluvial plain, current elevation nearly -360 m to -380 m, was formerly
located at the bottom of the Dead Sea and is dry land since an unknown time. It is now mainly used for
market gardening, and, for irrigation of the plants, water flowing from Wadi Ibn Hammad and
surrounding springs is stored in some man-made pools in the area.

Khalil (1992) published the geological information of the area (geologic map sheet Ar Rabba at 1:50000
125   scale). The bedrock underlying the alluvial plain is not exposed, but on structural grounds it probably
comprises limestone (some dolomitic or silicified), marl, chalk, and phosporite of the Ajun and Belqa
Groups of Late Cretaceous (Turonian – Campanian) age, and possibly also sandstones of the Ram and
Kurnub Groups of Cambrian and Early Cretaceous ages, respectively. The depth to bedrock under the
alluvial fan is unknown. West of Ghor Al-Haditha, the Lisan peninsula rises in the Dead Sea and uplifts at
130   a rate of nearly 9 mm/year by salt diapirism related to an underlying Usdom evaporate formation of Plio-
Pleistocene age (Taqieddin et al., 2000, Fiaschi et al., 2017). The alluvial plain consists of semi-
consolidated sands and gravels, interbedded with layers of silt, clay and marl (El-Isa et al., 1995,
Sawarieh et al., 2000), all of which are considered part of the lacustrine Lisan Marl Formation of Late
Pleistocene age. This sedimentation mixture was also observed during the survey in shallow outcrops of
135   1-2 m depth along new water pipeline constructions in the whole area, and at the flanks of up to 20 m
deep young sinkholes. The alluvial plain also comprises younger, unconsolidated alluvial gravels and
sands, especially around the modern wadi outlets. Together with the interbedded marl, evaporites, silt and
clay layers exposed in the adjacent mud flat (former Dead Sea bed), these younger semi-poorly
consolidated materials likely correspond to the Ze'elim Formation of Holocene age (Abou Karaki et al.,
140   2016)

2.1 Borehole information

Two boreholes (BH1 and BH2) were drilled at the Ghor Al-Haditha investigation site in January-
February of 1995 (**Fig. 1b**), and the drillings and sample analyses were firstly described in a report of El-
Isa et al. (1995). Bodet et al. (2010) reported two additional boreholes (**Fig. 1b**) from 2006, but without
145   further descriptions and not mentioned in other reports and publications. **Figure 2** shows the borehole
lithology of BH1 and BH2 based on a detailed microscopic analysis of cuttings (El-Isa et al., 1995).
There, the lithology is described as an alternating sequence of sand and gravel, with a "silt and clay" bed
at the bottom down to 51 m and 45 m depth, respectively. Nothing is mentioned about a massive salt
layer.

150   Several papers have subsequently presented lithologic cross sections for the Ghor Al-Haditha sinkhole
area, in which a thick (>2-10 m) pure salt layer is postulated to lie at between 30 m and 45 m depth below
the surface (e.g., Taqieddin et al., 2000, Frumkin et al., 2011, Ezersky et al., 2013 a,b,c, Ezersky et al.,
2017). The abovementioned boreholes, the reported depths of which vary from one paper to another, are
used to support this finding, although no detailed descriptions of the boreholes, no details about the

155 drilling method used, and no lithologic bars are provided. Because the indication of possible massive salt

layers is important for comparison with our results, we point to these inconsistencies here.
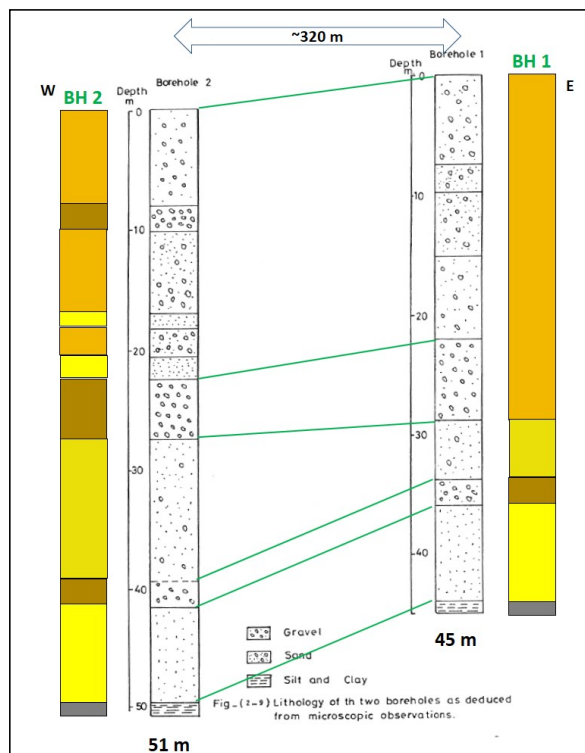
Figure 2: Lithologic columns of the boreholes BH1 and BH2 from microscopic analyses, referenced to their surface elevation (black and white columns are originals of El-Isa et al. (1995)). The coloured, generalized columns are used for the figures of this paper. The main dip tendencies of the units toward the west are visible by the green connecting lines. The annotated borehole depths below the columns follow the written text in El-Isa et al. (1995).

2.2 Previous geophysical surveys

180 Numerous, unpublished studies were carried out in the Ghor Al-Haditha area by the Ministry of Energy

and Mineral Resources (MEMR), Jordan (until 2014 the Natural Resources Authority, NRA) subsequent

to the first occurrence of the sinkholes (Sawarieh, pers. comm., 2013). Early refraction seismic

experimentss that used standard compression wave (P-wave) techniques were conducted in August-

December 1994 by the University of Jordan (El-Isa et al. 1995, blue lines in **Fig. 1b**), combined with first

185 hydrology and other geophysical studies. The equipment used is only poorly documented, seismic source

was a 7 kg sledgehammer. Then, hydrology and hydrochemistry work was accompanied by extended

seismic refraction (orange lines in **Fig. 1b**) and ground penetration radar (GPR) surveys in February 1999

(Sawarieh et al., 2000, Abueladas and Al-Zoubi, 2004). Seismic equipment was a 350 kg weight drop

source and a Bison Geopro 8024 24-channel recorder (10 m geophone interval). The refraction seismic

190 surveys indicated the thickness of the alluvial deposits of more than 70 m, a possible salt intrusion body

below (at least 70 m deep) at one profile location (profile 5 of Sawarieh et al., 2000, **Fig. 1b**), and also

sinkhole-causing cavities at relatively shallow depth (less than 20 m). Except the one location suspected for a salt intrusion body, the seismic velocity of the deepest refractor below 40-50 m depth was reported to vary from 2245 ms⁻¹ to 3300 ms⁻¹ in all profiles, and seismic velocities above this are in general less

195   than 2500 ms⁻¹. Unfortunately, the acquired seismic data of the 1994 and 1999 campaigns are irrecoverable.

Soon after the 1999 surveys, Batayneh et al. (2002) applied GPR to assess the potential of sinkholes of the Ghor Al-Haditha area and to determine the location of the filled sinkhole features within relatively dense and more resistive materials. Barjous et al. (2004) carried out a FDEM (Frequency Domain

200   Electromagnetic) survey, supplemented by DC resistivity methods (Wenner and Dipole-Dipole arrays), and conventional geological mapping techniques. During this work a systematic EM survey was applied on the Wadi Ibn Hammad alluvial fan.

More recent investigations carried out between 2005 and 2008 used a multi-method approach of transient electromagnetic (TEM) sounding, magnetic resonance sounding (MRS), GPR, and electric resistivity

205   tomography (ERT) (Camerlynck et al., 2012). In 2007, these included also a seismic survey along 4 profiles targeted to combined reflection, refraction tomography, and Multi Channel Analysis of Surface Wave (MASW) data analysis (e.g., Dhemaied, 2007, Bodet et al., 2010, Keydar et al., 2011, Ezersky et al., 2013a, magenta lines in **Fig. 1b**). For this seismic survey, a Geometrics recorder with a 24-channel geophone (4.5 Hz resonant frequency) spread in 5 m intervals and a sledgehammer source (mass not

210   reported) was utilized. MASW results are published in Bodet et al. (2010) (profile 3) and Keydar et al. (2011) (profiles 3&4). MASW results and interpretations of profiles 3 and 4 are published in Ezersky et al. (2013b), Ezersky and Frumkin (2013), and Ezersky et al. 2017. The limit of reliable depth penetration was reported as 60 m (maximum Half Space Depth), following the empirical formula $Z_{max}=0.5L$ of Park et al. (1999) and Rix and Leipski (1991), where L is the total source-receiver spread length of 120 m.

215   Results of profile 3 (magenta line 3 in **Fig. 1b**) show shear wave velocities of mainly less than 400 ms⁻¹ from surface to Z_{max}, while profile 4 (magenta line 4 in **Fig. 1b**) images a high velocity layer of more than 800 ms⁻¹ from nearly 30 m depth to Z_{max}, which was interpreted as the shallow salt layer. A reflection seismic analysis result of profile 4 in Ezersky and Frumkin (2013) shows no reflection response of the proposed shallow salt layer, however. Refraction tomography analysis results are reported to be of

220   insufficient resolution (Camerlynck,et al., 2012) and are later on shortly mentioned in Ezersky et al. (2017) only.

Three further MEMR geophysical surveys undertaken in 2009 and 2010 with GPR, Electrical Resistivity Tomography (ERT) and Time Domain Electromagnetic (TDEM) with NanoTEM technique, provide the most recent information about the sinkhole area in Ghor Al-Haditha (Alrshdan 2012). These newer results

225   depict geological and groundwater conditions, the salt-to-freshwater interface, and the limits of safe and vulnerable zones. Alrshdan (2012) also discusses the mechanism of sinkhole formation suggesting that the freshwater inflow acts as the major player, which dissolves cementing evaporite minerals and the fine materials within the alluvial fan, leaving weak alluvial layers and cavities which develop to sinkholes later on.

230   To shed more light on these different models and to provide an independent database for the detailed mapping of the postulated salt layer, its morphology, and synclinal structures expected at its top, we started high-resolution shear wave reflection seismic surveying in 2013 at Ghor Al-Haditha.

3. Shear wave reflection seismic equipment and survey

A shear wave landstreamer (Inazaki, 2004, Pugin et al. 2004, 2007, 2013) consisting of 95 transverse
235   horizontal (SH) geophones (10 Hz resonance frequency) in 1 m intervals was used as receiver unit, connected to a Geode (Geometrics Inc., 4 units of 24 channels each) recording system. Transverse horizontal (SH) waves were generated by the seismic micro-vibrator source ELVIS (Polom et al. 2011, Krawczyk et al. 2012, Polom et al. 2013). **Figure 3** shows the equipment in operation on site. The small size (nearly 1.5 m³) and weight (nearly 600 kg) of the whole equipment enabled air cargo transportation
240   to Jordan.

Figure 3: Photos of the shear wave seismic reflection acquisition campaign carried out in October 2013. (a) Wheelbarrow-mounted shear wave source system on asphalt pavement at start location of profile 2. (b) Recording car, towed land streamer and source during operation on profile 3. (c) Land streamer towed by the recording car during acquisition on profile 2. Colour paintings on the road surface were used for
245   location numbering along the profiles. (d) Sledge-mounted horizontal geophone in SH (particle movement perpendicular to profiling direction) configuration along profile 3.

The source signal (sweep) was set to 20-120 Hz (20-80 Hz during the survey extension in 2014) linear frequency modulated of 10 s duration (Crawford et al., 1960). Data recording was set to 12 s duration and
250   stored uncorrelated to enable processing of uncorrelated data later on, if required. In the field, vibroseis correlation processing was applied for immediate quality control. After initial tests on site, the source interval was set to 2 m to increase the statistical redundancy due to challenging, disturbed subsurface

conditions, noticeable by strong wave field scattering in the recordings. Typically, two records were gained at each source location and stored separately. Only during times of stronger wind disturbances the

255 number of records per location was increased to four. In the 2013 campaign, a total of 2011 records (9.34 Gb data volume) at 898 source locations were gained along 1.92 km of profile length. In 2014, 2000 records (9.14 Gb) at 1144 source locations were recorded along 2.1 km of profile length (see profile locations in **Fig. 4**).
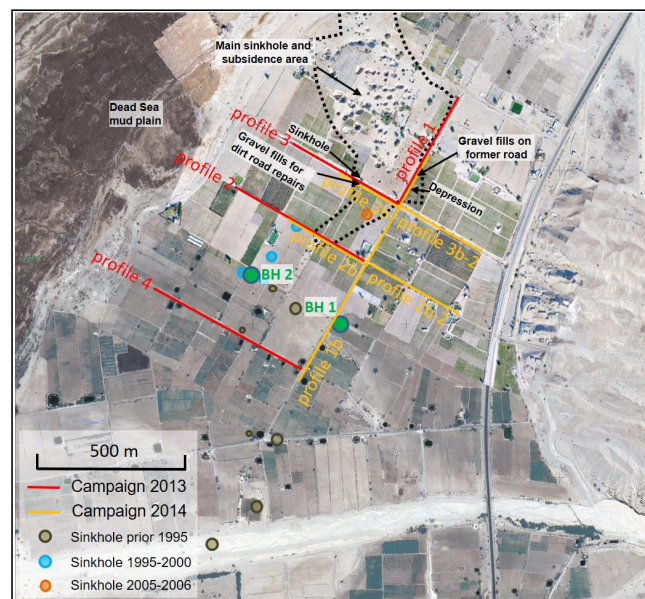
Figure 4: Map of the shear wave reflection seismic profiles acquired in 2013 (red lines) and 2014 (yellow
260 lines). Green circles denote the locations of the boreholes made in 1994 (according to report of El-Isa et al. (1995)). Older refilled sinkholes are denoted by brown circles (after El-Isa et al. (1995)), blue circles (after Sawarieh et al. (2000)), and orange circle (after Bodet et al. (2010)). The dotted black polygon marks the updated outline of the main sinkhole and subsidence area after Al-Halbouni et al. (2017).

265 A variable split-spread source-receiver configuration was applied to enable geometry optimization for the detection of dipping structures, and to facilitate workarounds due to obstacles in the profile track. To reduce the proportion of Love surface waves during recording, profiles were carried out mostly either on asphalt paved roads or on dirt roads covered by compacted gravel, so that high shear wave velocities at the surface disable the excitation of Love surface waves. In 2013, geodetic surveying of the profile tracks
270 was performed by using a handheld GPS system. Without differential GPS corrections, the final positioning of the profiles from the 2013 campaign required laborious optimizations by manual corrections based on the known distances along the receiver units. Reliable elevation data could not be restored. During the 2014 campaign, the positioning method was improved by using a Differential GPS system, leading to precise elevation data of 10 cm horizontal and 15 cm vertical error.

275   All seismic data recorded were checked and pre-processed in the evening of each recording day by using the VISTA 10.028 (GEDCO Inc., Calgary, CA) seismic data processing software on a notebook computer (DELL Precision M65) for quality-control purposes and a first interpretation. Detailed inspections of correlated raw records showed strong Love wave scattering on profiles 1 and 3 that indicated a low velocity layer close to the surface, even though the dirt road construction at profile 3 was modified some

280   years ago by gravel infill after a heavy damage caused by sinkholes and related subsidence.

Selected record examples along profile 1b illustrate the typical range of signal propagation responses at the Ghor Al-Haditha site (**Fig. 5**).
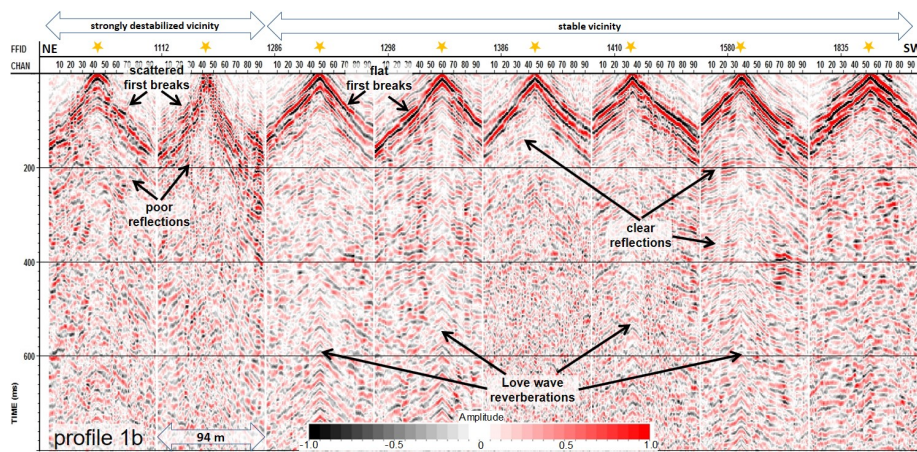
Figure 5: Examples of recorded shot gathers (AGC of 220 ms window, amplitude scaling and bandpass

285   filter (18-20-78-82 Hz) applied) in time domain along profile 1b. The positions of the seismic source are labelled by orange stars. FFID denotes the record number along the profile, CHAN denotes the geophone number along the landstreamer unit. Arrows at top denote the condition of the ground surface observed along the profile. In the NE, close to the sinkhole affected area, first break and reflection signals are weak due to the strong wave scattering in the subsurface caused by material loosening and cracking. The

290   situation improves towards SE, where no sinkholes or other subsidence features were present during profiling and the road surface was in good condition.

In the Northeast sector of the profile, close to the main sinkhole area, a typical scattering of the wave propagation is visible. The wave propagation behaviour is mostly asymmetric regarding the receiver

295   distance to the source position, which indicates heterogeneous subsurface structures. In the middle sector, even though an asphalt surface pavement of apparently continuous integrity, Love wave propagation was partly indicated (note area of Love wave reverberations marked on **Fig. 5**), probably caused by poor road construction. In the Southwest sector, clear reflection events were detected already in the single recordings. Along profile 2b-2 (**Fig. 6**) selected record examples show a better data quality compared to

300   profile 1b: flat first breaks and a range of clear reflection events occur. This is surprising, because the

road quality along profile 2b-2 did not differ to that of the southwest sector of profile 1, and both roads are of obviously similar age.
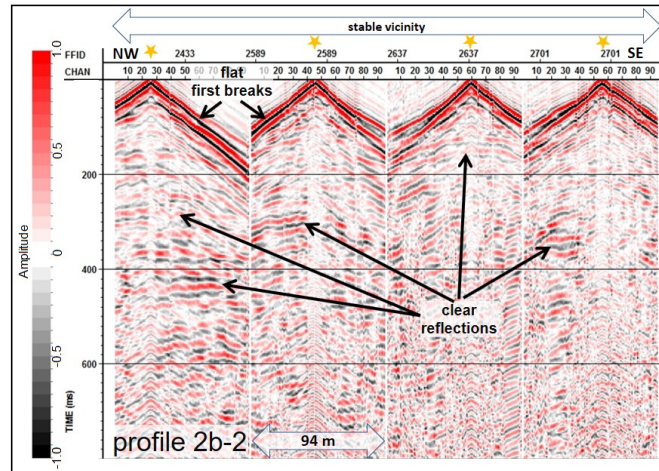
Figure 6: Examples of recorded shot gathers (AGC of 220 ms window, amplitude scaling and bandpass filter (18-20-78-82 Hz) applied) in time domain along profile 2b-2 (labelling as in **Fig. 5**). Good signal quality of first breaks and reflections mirrors a rather unaffected signal propagation in the subsurface, which correlates to the sinkhole-unaffected vicinity at surface. Reflection signals up to 400 ms in time represent layer responses from 70 m depth (applying 350 ms^{-1} shear wave propagation velocity).

4. Data processing

Reflection imaging was carried out by following a general processing sequence described by, e.g., Krawczyk et al. (2012) and Polom et al. (2013). The main data processing flow of the first iteration consisted of Vibroseis Correlation, Vertical Stacking of records, Geometry Installation, Amplitude Scaling, Bandpass Filter, Frequency-Wavenumber (FK) Filter, Interactive Velocity Analysis, Common Mid Point (CMP) Stacking, parallel applied Frequency-Space (FX) Deconvolution and Finite-Difference (FD) Migration. Subsequently, depth conversion was applied by using a mean 1D velocity function. Background of data processing applied is reported in Aki and Richards (1980) and Yilmaz (2001).

Since Love wave reverberation patterns are a widely observed disturbance effect in the whole data set (c.f., **Fig. 5**), elimination of such patterns was one of the main processing steps undertaken to enhance the desired reflection response. This required several iterative loops during the main processing sequence to improve the final result. The main data processing was carried out in two iteration sequences mainly by using VISTA 10.028 (GEDCO Inc., Calgary, CA) seismic data processing software. The first sequence was carried out to establish the main database and to extract the main structures in the data. In the second iteration sequence, the time section results were used to improve the processing flow in detail towards the specific reduction of imaging artefacts and to stabilize the processing velocities for later use during depth conversion. It included reduction of harmonic distortions in the near source area and Vibroseis Spectral

325 Balancing (Pugin et al. 2009) in a Vibrogram transformation domain (Polom 1997). Furthermore, the results of the velocity analysis were improved to derive final depth sections by using a mean 1D velocity-time function (shown in **Fig. 7**) for all profiles. Because of these general improvements, some structures in the near surface down to 50 m became weaker than in the first iteration. This is a compromise result of combining shallow velocity results affected by wave propagation along irregular, non-straight ray paths

330 (due to the disturbed shallow subsurface structure) with more regular straight ray path responses from deeper levels (later travel times).

5. Resulting depth sections and structure correlations
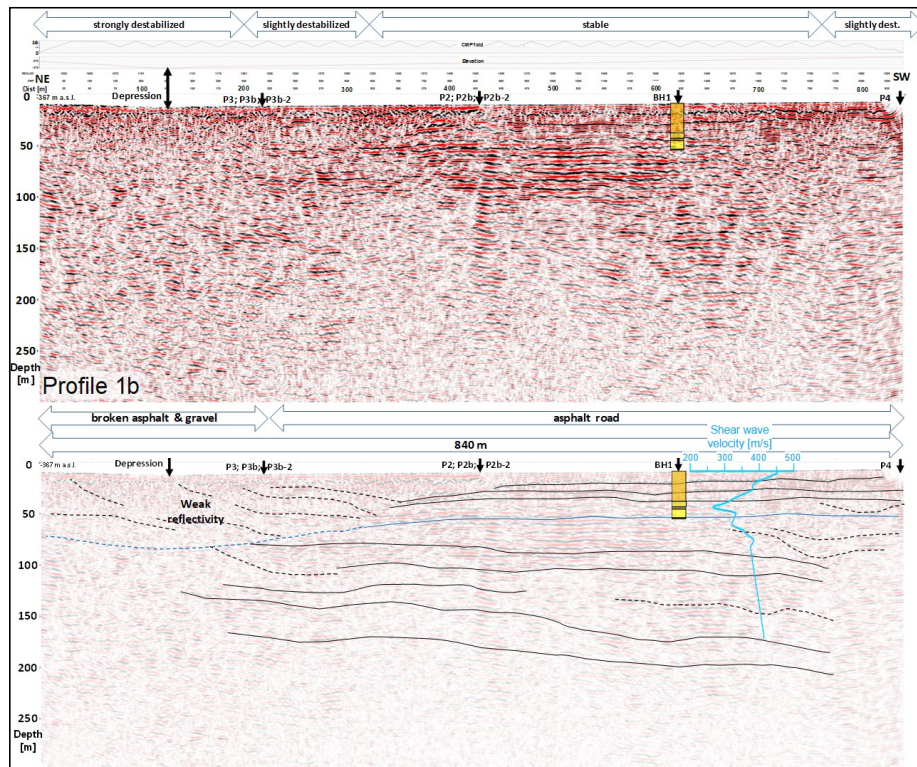
Figure 7: Resulting depth section of profile 1b after post stack FD time migration (top) and interpretation of the main structure elements (bottom). Arrow bars at the top of the upper image denote the surface

335 instability/stability as observed along the profile, while arrow bars below denote the road surface situation along the profile and the profile length. Black arrows at top indicate joints to crossing profiles. The lithology of borehole BH1 is projected from 10 m distance perpendicular into the profile. The interpreted top of the "silt and clay" layer in BH1 is shown as the blue line along the profile, since it is the first layer detected at depth that is prone to subrosion. Also shown is the 1D shear wave velocity-depth function

340 derived from seismic data in this area; this function was used for time-to-depth conversion of all profiles.

The main NE-SW-trending profile 1b has transparent and strongly layered segments between ground surface and 200 m depth (**Fig. 7**). The depth section of profile 1b refers to a reference level of -367 m a.s.l. and it includes annotations of joints to the other profiles, remarks about the surrounding area (top),

345   and information on the road construction (bottom). The location of borehole BH1 which is nearly 10 m SE of the profile is projected perpendicularly into the profile and shown with a simplified lithology (see **Fig. 2**). The mean 1D velocity function used for time-to-depth conversion was derived from the reflection seismic data and is given as interval velocity in depth (Dix, 1955) beside the borehole BH1. It shows estimated shear wave velocities in the range of 250-450 ms^{-1} down to depths of about 170 m. Finally, the

350   reflection amplitude responses throughout all seismic sections represent reflection coefficients of nearly 0.1 or less, indicating materials with relatively low contrasts in seismically-sensitive material properties (elastic parameters and density) and hence in shear wave seismic velocity.

The main area of sinkhole activity is located immediately northwest of profile 1 (see **Fig.4**). This activity has strongly affected the road construction along this part of profile 1b, northeast of its intersection with

355   profile 3 (**Fig. 7**). A depression with several fractures is visible here along the road surface (**Fig. 4**), but without any sinkhole activity until yet. In detail, this part of the road crosses the south-eastern limit of a major sinuous depression that runs down to the former Dead Sea shore and that hosts the smaller scale sinkholes (for details see Al-Halbouni et al. (2017)). Several gravel infills on the former asphalt surface in the past enable the usability of this part of the road. Further along profile 1b, to the southwest of its

360   intersection with profile 3, the road stability continuously increases. The road surface is essentially unaffected by subsidence along the area denoted as stable along the southwest half of the profile 1b. Within this stable area, from the intersection of profile 1b with profile 2 to the borehole BH1, a continuous reflectivity pattern is visible below 50 m reference depth (i.e. nearly 45 m below the ground surface). The top of this pattern nearly correlates with the depth of the „silt and clay" layer detected 44 m

365   below the ground surface in borehole BH1. The bottom of the nearly horizontal pattern reaches to nearly 100 m depth below reference level along much of the profile, although SW of the BH1 location the pattern extends downward to 230 m depth within a V-shaped structure. NE of the intersection of profiles 1 and 2, the pattern becomes weak and disappears NE of the intersection of profiles 1 and 3. Also SW of borehole BH1 the horizontal pattern weakens and bowl-shaped structures become more dominant.

370   Overall, the pattern widely correlates with the stable part of the road, where no sinkholes have occurred yet. Above this pattern, around the borehole BH1 location, nearly horizontal layers occur which show finer subdivided structures resolved down to meter scale. This finer layered structure also abruptly disappears NE of the intersection of profiles 1 and 2, i.e. as one approaches the main sinkhole area.

The combined depth sections of profiles 2 and 2b-2 are shown in **Fig. 8**. The profiles were both acquired

375   on asphalt road. Also shown in **Fig. 8** are the simplified lithological bars of boreholes BH1 and BH2 as projected perpendicularly into the profile plane from their true locations nearly 200 m to the SW (c.f., El-Isa et al., 1995). Due to this relatively large projection distance, the lithology bars may not precisely reflect the lithology in the profile plane. The sections show a nearly horizontal layering down to 50 m

depth below the reference level of -367 m a.s.l. in the SE part of the combined profile, which changes
380   laterally to less well organized but mainly NW-dipping structures in the NW part of the combined profile.
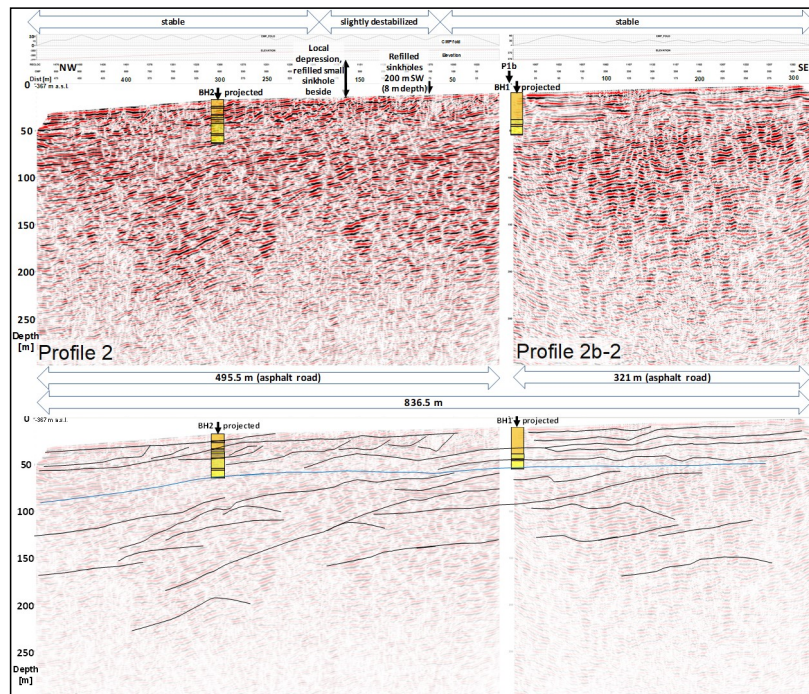
Figure 8: Resulting depth sections of combined profiles 2 and 2b-2 after post-stack FD time migration
(top) and interpretation of the main structure elements (bottom). For annotations see **Fig. 7**. Lithology of
boreholes BH1 and BH2 is projected perpendicular into the profile from 200 m distance, and therefore
may not show the precise layering signature. Except the top 40 m the main characteristics down to 200 m
385   show stacked sequences of NW-dipping reflectors, which are interpreted as NW-prograding alluvial fan
sequences. The interpreted top of the "silt and clay" layer in BH1 and BH2 is shown by the blue line.

Below 50 m depth the main structural dip is towards the NW and is divided into several dip sequences
visible down to nearly 250 m. Along profile 2, between profiling positions 75m and 200 m, there is a
390   slightly more disorganised seismic response above 50 m depth (i.e. from 30-35 m below the ground
surface). This is spatially associated with a local depression and related cracks in the road. At least one
sinkhole formed directly adjacent to this part of road prior to 2000 (Sawarieh et al., 2000) and was
subsequently filled in. Along profile 2b-2, at profiling position 125 m, a striking stack of bowl shaped
structures is visible from the surface down to nearly 75 m depth. Along this part of the profile and for at
395   least 300 m on either side of it (i.e. towards NE and SW) no sinkhole activity was reported in the past.
The combined depth sections of profiles 3 and 3b-2 are shown in Fig. 9. The boreholes BH1 and BH2 are
again projected perpendicularly to the profile plane, in this case over a distance of nearly 420 m from
their true positions further SW, and so they may only indicate a lithological tendency.

Figure 9: Combined depth sections of profiles 3 and 3b-2 after post stack FD time migration (top) and

400 interpretation of the main structure elements (bottom). For annotations see **Fig. 7**. Lithology of boreholes
BH1 and BH2 are projected from 400 m distance perpendicular into the profile, therefore probably not
showing the precise layer signature. The interpreted top of the "silt and clay" layer in BH1 and BH2 is
shown by the blue line. The centre part of the profiling track was repeatedly affected by recent sinkhole
activity directly beside in the NE. For farming access it was refilled with gravel along more than 250 m,

405 which was subsequently again affected by sinkholes and subsidence. This may cause the weaker
reflection signatures in the upper 50 m if compared to profile 2 (**Fig. 8**). The main reflection pattern
signature is similar to profile 2 and 2b-2, showing NW dipping events. In the SE of the profile a V-shaped
structure is visible close to surface, filled with nearly horizontal reflection events, which is interpreted as
a refilled channel side-cut. Due to the wide subsidence area NE of profile 3 the top of the "silt and clay"

410 layer (blue line) was continued to NW starting from profile 1b instead using the projection of BH2.

Profiles 3 and 3b-2 were acquired on a gravel farm track and on a gravel path, respectively, both close to
a parallel drainage channel. A 250 m long segment of the farm track along profile 3 was refilled
extensively in the past. The main area of sinkhole activity lies immediately northeast of this refilled

415 section of profile 3 (see **Fig. 4**), and indeed a recent sinkhole (formed in 2008) was located directly beside
the track during data acquisition.

NE of profile 3b-2 no sinkhole activity was reported in the past. Due to the different surface conditions, and probably caused by the sinkhole activity directly beside profile 3, these sections slightly differ in seismic signature. Profile 3b-2 shows some undulating layer structures of continuous amplitudes to 50 m

420   depth below reference datum (40-45 m below the ground surface), which change at the NW end of the profile to NW-dipping sequences. In the very SE part of the profile, a bowl-shaped structure sequence is dominating down to 80 m depth, but without any indication of deformation at the surface. Profile 3 shows mainly NW-dipping structural elements without significant amplitude variations, especially above 100 m depth. Only small bowl-shaped structures are visible.
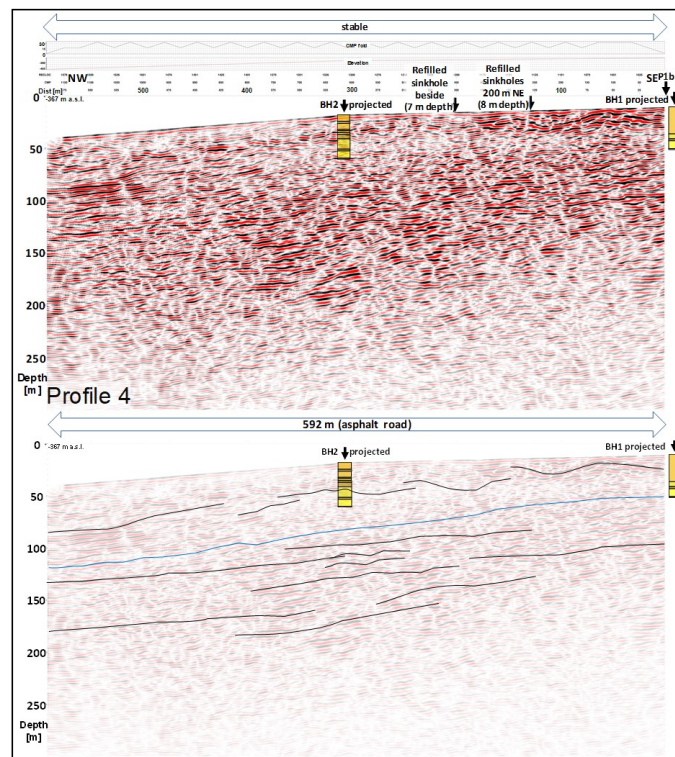
425   **Figure 10**: Depth section of profile 4 after post stack FD time migration (top) and interpretation of the main structure elements (bottom). For annotations see **Fig. 7**. Lithology of boreholes BH1 and BH2 is projected from 200 m distance perpendicular into the profile. In contrast to profile 2, more gently NW-dipping events are present to 150 m depth, indicating less transportation energy of the alluvial material or an apparent structure dip. The top of the "silt and clay" layer in BH1 and BH2 is interpreted by the blue

430   line. Bowl shaped signatures close to the surface in the SE indicate sinkhole-caused subsidence and/or refilled channel side-cuts. Significant reflection amplitudes of a stronger reflector pattern close to the NW end at nearly 90 m depth may indicate an evaporite-rich lense included in the alluvium-lacustrine deposits.

435   The depth section of profile 4 (**Fig. 10**), which again includes projections of boreholes BH1 and BH2
(both in reality located nearly 200 m NE of the profile plane), shows mainly slightly NW-dipping
structural signatures. Bowl-shaped structures are restricted to the top 50 m of the SE part of the profile,
which lies less than 200 m SW of where sinkhole activity was reported by El-Isa et al. (1995) and
Sawarieh et al. (2000) in the 1990-2000 decade. One sinkhole of 7 m depth was reported to have formed

440   beside the road prior to 1992. No surface damages were reported for the road track itself, however, and no
depressions, cracks or repairs were visible at the surface during data acquisition. At the NW end of the
section several continuous events of higher amplitudes occur nearly 50 m below the surface.

Figure 11 shows a 2.5D grid of the profiles shown in **Fig. 7-10** including the continuation of profile 1b
along profile 1.
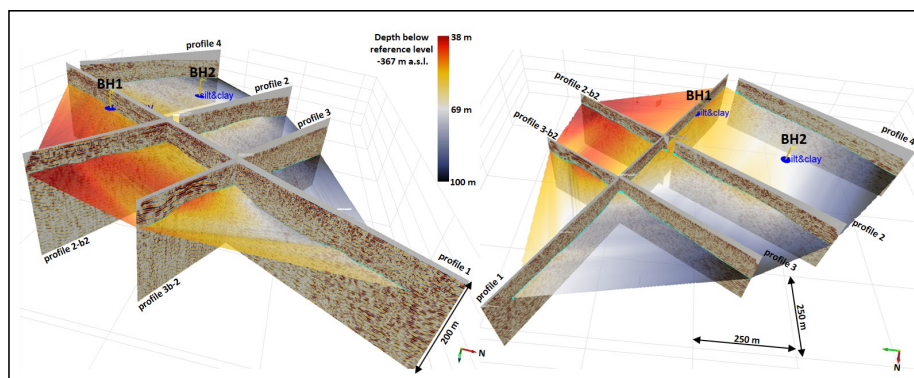
445   **Figure 11**: 3D representation of the 2.5D profiling grid (c.f., sections in **Fig. 7-10**, restricted to 200 m
depth (no vertical exaggeration). Boreholes BH1 and BH2 are included as yellow bars representing the
sand and gravel sequence above the detected „silt and clay" layer, the top of which is marked by a blue
disc along each well shaft. Light blue lines along the profiles mark the interpreted continuation of the top
of this layer starting from BH1 along profile 1 and subsequently continued to the crossing profiles. The

450   constructed horizon by triangular interpolation represents the derived top of the "silt and clay" layer
below the reference datum of -367 m a.s.l. based on the drilling and seismic results. At the deepest parts
towards the Dead Sea border the top of this layer reaches nearly -467 m a.s.l., which is 60 m below the
level of the current alluvium/mud-flat transition of -407 m a.s.l. calculated by Al-Halbouni et al. (2017).

455   Also integrated are the simplified columns of boreholes BH1 and BH2. The reference level at the section
top is -367 m a.s.l. The image illustrates that a direct projection of borehole BH2 to profiles 2 and 4 needs
to be carefully handled due to the projection distance of nearly 200 m. Nevertheless, the results of the
profiles 2 and 4 both show main structural dips towards NW, which fit the dip tendency of the lithology
detected in the boreholes (**Fig. 2**). Blue markers included along the borehole shafts in **Fig. 11** determine

460   the top of the „silt and clay" layer below the alluvium sequence consisting of gravel and sand. Since this
„silt and clay" layer is the only one detected in the lithology bars of the boreholes that is prone to act as
an aquiclude sensitive to subrosion, and it also fits the general structural dip, it was obvious that this layer

probably extends across the whole area. To interpolate the top of this layer in space (light blue colour in **Fig. 7-10**), it was traced from borehole BH1 along profile 1b and profile 1, from where it was further

465 continued to profiles 2 and 2b-2, profiles 3 and 3b-2, and profile 4, with respect to the perpendicular projection of borehole BH2 into the profiles 2 and 4. Subsequently, these layer continuations along the profiles were triangularly interpolated in space to get an impression of the probable layer extent and topography. Regarding the lithology of boreholes BH1 and BH2, the constructed horizon represents the estimated base of the upper alluvial gravel and sand unit. The lithology of this upper alluvial unit shows

470 no sequence prone to subrosion, and neither the borehole lithology nor the seismic reflection responses give indications for any included massive salt layers or extended salt lenses. Therefore, the subrosion as origin of the sinkhole process on the exposed alluvial fan is estimated to occur mainly below this constructed horizon within the area of the seismic survey. The deepest part of this constructed horizon reaches -467 m a.s.l towards NW, which is 60 m below the level of the current alluvium-to-mud-flat

475 transition of -407 m a.s.l. at the former shoreline of the Dead Sea in the 1960s (as calculated by Al-Halbouni et al. (2017)). It therefore represents a different subrosion level to the present mud-flat surface, which indicates that alluvium and "silt and clay" sequences may lie below the presently exposed mud-flat.

6. Discussion

480 The shear wave reflection seismic survey acquired at the Ghor Al-Haditha sinkhole site in 2013 and 2014 was the first comprehensive shallow seismic investigation of the sinkhole phenomena area since the refraction seismic investigation campaigns carried out by El-Isa et al. (1995) and Sawarieh et al. (2000), respectively. The results presented here show the advantageous imaging capabilities of the method regarding high-resolution structural analysis and depth penetration compared to common refraction

485 seismic methods or common P-wave reflection analysis. In this section, we discuss firstly the general outcomes of our application of the S-wave reflection method to an alluvial fan setting and secondly the implications for the nature of processes leading to sinkhole development at the Ghor Al-Haditha site.

6. 1 The application of the shear wave reflection seismic technique to alluvial fan setting

The S-wave reflection method is especially advantageous in the area close to the Dead Sea border,

490 because wave propagation is restricted to the matrix only, and so it is not affected by the pore space content, whether that is air in the shallow unsaturated zone or fresh- or salt water in the deeper parts below the ground water level. Therefore the groundwater level itself does not act as a physical interface during wave propagation, as it is in general the case for common P-wave methods. In the S-wave profiles acquired in the area, no influence and no response of the ground water level to the wave propagation was

495 detected. Furthermore, wave propagation velocities of S-waves (Vs) are in general significantly smaller than those of P-waves (Vp). The Vp/Vs-ratio ranges from nearly 1.7 for an ideal elastic medium (e.g. perfect consolidated rock) to more than 10 (Yilmaz, 2015) for unconsolidated sediments (e.g. Holocene

alluvium and soft clays). This leads to a significantly improved resolution when using S-waves, depending on the grade of matrix consolidation. In the case of the Ghor Al-Haditha site, this results into a

500 resolution improvement factor of 8-10 below the ground water level, when one postulates a similar seismic signal frequency bandwidth for P- and S-waves.

The success of the application to the alluvial fan setting at Ghor al-Haditha is seen in the well-resolved shallow subsurface structure imaged in the seismic profiles, which show in general mainly NW dipping (i.e. lake-ward-dipping) reflectors typical of a prograding alluvial fan sequence into a lacustrine

505 environment. The internal structure is complex and includes typical fan-delta elements such as topsets, foresets, and indications of bottomsets. Especially profile 2 in **Fig. 8** shows typical dip structures of a Gilbert-type delta (Gilbert, 1885). Intercalated, more-horizontal structures indicate lacustrine deposit layers. The topset structures, the intercalated lacustrine deposit layer and the dip directions fit the lithology of both boreholes BH1 and BH2, which show NW-dipping alluvial sand and gravel above an

510 obviously lacustrine-type deposit denoted as "silt and clay" (**Fig. 2**). Below the blue line (**Fig. 7-10**), stacked foreset structures dominate in profiles 2-4, connected to bottomset structure indications in the NW. Due to the absence of borehole information for depths greater than 51 m below the ground surface, more detailed interpretations remain speculative and require further investigations. With respect to the fluctuations of the Dead Sea level (Bookman (Ken-Tor) et al., 2004) in the past, several levels of included

515 lacustrine-type deposits in the fan architecture are most probable and these may have a complex distribution in three dimensions. For instance, the refill of eroded alluvial channels on the fan surfaces by lacustrine deposits may be a mechanism for inclusion of soluble fine material in the alluvial fan structure. Furthermore tectonic induced level variations of the whole fan structure, caused by the sinistral transform fault movement, cannot be excluded.

520 Since wave propagation is controlled by the matrix only, effects of grain size coupling play a key role in the wave propagation of S-waves in contrast to P-waves. In contrast to P-wave velocity, which usually increases with depth in the case of a fluid-saturated pore space, S-wave velocities often decrease with depth, e.g., if the grain cementation reduces or the pore pressure increases with depth, respectively, as both factors result in reduced grain contacts. A further reason for velocity function decrease with depth is

525 the influence of a high-velocity layer at the surface, which is the case operating on an asphalt road surface. This effect is visible in the 1D velocity-depth function in **Fig. 7** in the range 0-10 m below ground surface. Diminished grain coupling can also arise from mechanical damage, e.g. by fracturing, subsidence and subrosion, which leads to breaks in the direct (geometrical) wave paths. In contrast to P-waves, where such breaks may be short cut due to the wave propagation through the pore fluids,

530 decoupling between grains causes additional paths for S-waves, leading to enhanced wave energy scattering and an apparent velocity reduction.

In the Ghor Al-Haditha data, enhanced wave energy scattering was observed in areas close to sinkhole activity, leading to transparent zones of weak reflectivity in the seismic sections (e.g., **Fig. 7, 9**). In the northeast part of profile 1b in **Fig. 7**, the zone of scattered reflections is imaged up to 60 m depth below

535 the reference level of -367 m a.s.l. (i.e. nearly 50 m below the ground surface), indicating the depth range of the destabilized alluvium. Profile 3 in **Fig. 9** shows the continuation of this low reflectivity zone to 70

m depth below the reference level (i.e. nearly 50 m below the ground surface) in the centre of that profile. Beside the transparent zones of strong wave field scattering, buried syncline structures imaged in profiles 2b-2 (**Fig. 8**), 3b-2 (**Fig. 9**) and profile 4 (**Fig. 10**) are in the depth range of 30-60 m below ground

540   surface. These synclines probably indicate ancient or recent subsidence by sinkhole activity caused by subrosion below the syncline centres at different horizons. The structures are targets for time-lapse monitoring by shear wave reflection seismics in the upcoming years to evaluate changes in the reflectivity response in detail.

The effect of apparent velocity reduction was also observed, leading partly to irregular interval velocities

545   values less than zero. Whereas this velocity problem is of minor importance for the CMP stacking, processing the velocity functions of the individual profiles required careful handling during the time-to-depth conversion. Since the discrepancies could not be eliminated due to missing additional velocity information, e.g. by well logging, the final depth conversion was carried out by using a stabilized 1D velocity function for all profiles (**Fig. 7**), derived as mean function from profile parts with sufficient

550   reflection responses. Therefore, the resulting depths have to be handled with an estimated error range of up to 20%.

As well known in hydrocarbon exploration and shallow seismic operations using the seismic refraction, reflection, borehole and other seismic methods, there are no stand-alone seismic properties that enable the detection of the lithology or the grain size of a layer. This holds also for other geophysical methods and

555   their combinations. Such conclusions can only be reached if seismic results are calibrated by comprehensive borehole coring in the investigation area. Since the borehole descriptions of BH1 and BH2 are based on the analysis of cuttings only, precise lithology depths and the information about grain size derived from the boreholes are in principle poor, and no information is available below the borehole bottoms due to the missing well logging. The alluvial fill rate can be estimated relatively by the borehole

560   lithology profiles and by the seismic structure dips, but must be handled with care since geochronological data are limited and the area is close to an active, main sinistral strike-slip transform fault. It is to be expected beside the lake level variations that tectonic overprints may have changed the whole sedimentation structure over time, even though there was no main fault structure detected in the seismic data.

565   In summary, the S-wave reflection seismic method achieved advantageous high-resolution imaging results of the alluvial-lacustrine deposit structure at the Ghor Al-Haditha sinkhole site, which are superior to common near-surface seismic investigation methods. The favourable velocity-frequency relationship of the resulting wavelets and the absence of pore fluid effects enabled a meter-scale resolution and a nearly 200 m penetration depth. Furthermore, and unlike the refraction method, the shear wave reflection

570   method is independent of an obligatory increasing velocity-depth function. In the case of the sinkhole affected subsurface structure at Ghor Al-Haditha, where strong vertical and lateral subsurface inhomogeneity occurs, it is not free from shortcomings, and, similar to other geophysical methods, it requires borehole calibration to verify precise depth imaging, especially.

6. 2 Implications of the shear wave reflection seismic results for sinkhole formation

575 Combining the reflection amplitude responses and the detected borehole lithologies of BH1 and BH2 (**Fig. 7-10**) results in no indication for an extended massive salt layer of several meters thickness in the depth range 35-52 m below the ground surface, as proposed e.g. by Taquieddin et al. (2000), Frumkin et al. (2011), Ezersky et al. (2013 a,b,c) and Ezersky et al. (2017). If a massive salt layer of thickness more than 2 m would be present in the shallow subsurface down to 200 m depth, which is our estimated limit of

580 stable imaging, this would result in strong seismic reflection responses in our profiles. A reflection coefficient of nearly 0.5 has to be expected for an alluvium-salt interface, if one assumes mass densities for alluvium (~1900 kgm^{-3}) and salt (2200 kgm^{-3}) and if one assumes the mean shear wave velocity range of 250-450 ms^{-1} in the alluvium, as detected during data processing, and of at least 1000-1600 ms^{-1} for a massive salt layer, as reported by Ezersky and Livne (2013) for the boreholes MN-5E and EB-3E at the

585 western Dead Sea shore. In contrast, the reflection amplitude responses visible below 52 m depth are similar to the reflection amplitude responses above 52 m depth, which represent reflection coefficients of nearly 0.1 and less. We also find no indication of anticlinal structures, as has to be expected from salt diapirism or salt pillows below 52 m depth. Finally, there is no structure or amplitude indication for a hard rock basement below the alluvial-lacustrine sequence as imaged in the profiles down to depths of

590 about 200m. Such low Vs values and reflection coefficients are typical for poorly-consolidated alluvial and lacustrine siliciclastic deposits, and are consistent with the existing borehole information at Ghor Al-Haditha. Similar low Vs velocities for alluvium and silty clay layers (Vs: 100-600 m/s) were reported at the western Dead Sea shore (e.g. Ezersky and Livne, 2013, Gorstein and Ezersky, 2015, Ezersky et al., 2017), as proven by in-situ tests in logged boreholes and laboratory tests on related samples.

595 The previously-derived MASW results at the Ghor Al-Haditha site (Bodet et al., 2010, Keydar et al., 2011, Ezersky et al., 2013b, Ezersky et al., 2017) also show Vs of 200-400 ms^{-1} from surface to nearly 50 m depth (magenta profile 3 in **Fig. 1**) and to nearly 30 m depth (magenta profile 4 in **Fig. 1**). Assuming a mean Vs value of 300 ms^{-1} and taking into account the 4.5 Hz low frequency limit of the geophones used for the MASW survey (see the fundamental mode low frequency limit in Ezersky et al. (2013b), **Fig. 4c**),

600 such low Vs values restrict the data-driven maximum Rayleigh wavelength to 62 m (V$_R$ ~0.93 Vs). This results to a maximum MASW investigation depth of 31 m according to e.g. Park et al. (1999), Rix and Leipski (1991), Park and Carnevale (2010), in contrast to the rule-of-thumb maximum depth estimation of 60 m (0.5 of the spread length) based on the survey spread length of 120 m. The significance of the high velocity layer of Vs > 800 ms^{-1} reported to lie below 35-40 m in MASW profile 4, which is the only

605 reported S-wave evidence for the proposed shallow salt layer at the Ghor Al-Haditha site, must therefore be handled with precaution. The strong lateral Vs inhomogeneity reported (Bodet et al., 2010) is additionally in contrast to the required 1D layer structure along the spread; such inhomogeneity is well known to cause impaired inversion processing results for the MASW method (Forbriger, 2003).

Due to the significant difference in propagation velocities of P- and S-waves, the S-wave velocity results

610 in this study are not comparable to the P-wave refraction velocity results of the previous studies of El-Isa et al. (1995) and Sawarieh et al. (2000). El-Isa et al. (1995) detected a deepest refractor layer of Vp max.

2500-3300 ms⁻¹ at 40-50 m depth in nearly all of their profiles. In the profiling tracks which were repeated by Sawarieh et al. (2000) using a similar acquisition configuration, max. P-wave refraction velocities Vp of 2500 ms⁻¹ and 3130 ms⁻¹ were detected for similar depths, but predominantly the detected

615 velocities were around 2150 ms⁻¹ in nearly 40-50 m depth. In only one of 24 profiles (No. 5, **Fig. 1**) of Sawarieh et al. (2000), in the northwest outside the study area of El-Isa et al. (1995) and close to profile 3 of our study, Sawarieh et al. (2000) detected a P-wave velocity of 3948 ms⁻¹ in 70 m depth, which was interpreted as a salt diapir. Directly beside their profile 5, in their profile 4 (**Fig 1**), Sawarieh et al. (2000) detected a maximum velocity of 2245 ms⁻¹ in 40 m depth. The area of profile 4 was subsequently affected

620 since 2000 by massive sinkhole activity and subsidence, which prevented further investigation, whereas the area of profile 5 remained unaffected until today (see **Fig. 1** and **Fig. 4**). For the Ghor Al-Haditha site, these observations of sinkhole development are in direct contradiction to predictions of the salt layer edge model as suggested e.g. in Ezersky (2017) and as based on the abovementioned P-wave refraction velocities.

625 Overall, the P-wave velocities reported for the depth interval of 40-60 m in past studies are by themselves not indicative of a laterally extensive, thick, massive salt layer at that level. Regarding borehole-defined salt layers on the western shore of the Dead Sea, the overview by Ezersky et al. (2017) notes that P-wave velocities for adjacent alluvial and lacustrine sediments range from 2000-2900 m/s, while P-wave velocities for the salt layers themselves range from 2900-4500 m/s. The velocities reported for Ghor al-

630 Haditha area in the 30-60 m depth level thus overlap with the mid-upper end of the range expected for semi-consolidated, water-saturated, alluvial or lacustrine deposits and with the lowermost end of the range expected for compacted salt, and are thus lithologically ambiguous. Moreover, the interpretation of such velocities in terms of a massive salt layer is not supported by borehole data available at Ghor Al-Haditha for the relevant depth interval.

635 Another hypothesis in discussion (Ezersky et al., 2017) states the shallow salt layer proposed previously at Ghor Al-Haditha could not be detected in our study, because it was already completely dissolved in the period 2006-2013 - i.e. before our survey. This hypothesis would additionally postulate that the lithology description of BH1 and BH2 carried out in 1994 may have been flawed, because any salt encountered was probably immediately dissolved by the freshwater bore fluid during the drilling process and so did not

640 remain in the analyzed cuttings. This latter postulation cannot be assessed since details of the drilling operation and especially the bore fluid are not documented in El-Isa et al. (1995) or elsewhere. Nonetheless if the proposed >10 m thick shallow salt layer (e.g. Taquieddin et al., 2000, Ezersky et al., 2013) was completely subroded in 2006-2013 from the surrounding area of BH1 and BH2 (see **Figure 1b**), subsequent extensive sinkhole development as well as more distributed subsidence of several meters

645 have to be expected in this area. Actually, this was not the case; the area has been essentially stable since 2006 (see **Fig. 4** here and **Fig. 4** in Ezersky 2013a).

The most significant horizon in both boreholes for which documentation exists is the "silt and clay" layer with its top below ground surface at 43 m in BH1 and 49 m in BH2, respectively, because this is the one detected in the boreholes that is most prone to subrosion. The drilling of boreholes BH1 and BH2 both

650 had been stopped after nearly 2 m within this layer because it was interpreted as base of the sand and

gravel sequence, and because it was supposed to act as aquiclude regarding hydrogeological aspects (El-Isa et al., 1995). Profile 1b (**Fig. 7**) shows a change of the main reflection pattern at the location of borehole BH1 from nearly the top of this layer (ca. -420 m a.s.l., 50 m below surface) to 110 m below reference depth (ca. -470 m a.s.l., 100 m below surface). So it is obvious that the thickness of this layer is

655 either more than 2 m, or that this layer is part of a stacked sequence including several „silt and clay" layers below. Since the depth range of the "silt and clay" layer was always below the Dead Sea level, the sedimentation of this layer occurred in the lacustrine evaporite-rich environment of the Dead Sea during the last 10 ka BP (Bookman et al., 2004). In analogy to exposures of lacustrine deposits visible in the sides of 1-8 m deep freshwater channels that were carved recently into today's mud plain (e.g. Al-

660 Halbouni et al., 2017) there may be also thin evaporite layers (<1 m thick) embedded in this "silt and clay" sequence below the alluvial plain.

The mineralogy of the clay material in the „silt and clay" layer in BH1 and BH2 was not determined by El-Isa et al. (1995). The clay material was only described to be of green colour, this would be an indication for illite (also called French clay), which is typically described to be of dark olive-grey colour

665 and contains portions of potassium and water. Sawarieh et al. (2000) described several fine material outcrop sequences in sinkholes at the Ghor Al-Haditha site as marl and clay both of greenish grey colour. This is similar to the composition of Dead Sea mud sampled at the eastern shoreline by Khlaifat et al. (2010) which typically consist of >40% fine carbonates (aragonite, calcite, CO_2), up to 20% clay, 20% quartz, and additionally halite, water and further minerals in fractions. The absence of another source for

670 such fine material layers forces the assumption that the majority of silty-clayey fine material layers included in the alluvial fan is Dead Sea mud, probably in different mineral compositions depending on the environmental conditions during sedimentation. Due to the high content of included marl and evaporites, all these layers are prone to dissolution and subrosion instead of acting as an aquiclude consisting of pure clay. Such kind of dissolution and erosion processes can be observed today in the mud

675 plain all around the Dead Sea, where freshwater channels from the highlands or springs meet the Dead Sea shoreline, forming erosion channels in the mud plain, both on the surface and in the subsurface (Al-Halbouni et al., 2017).

This solution process may be in places amplified by a physical effect well known for the so-called "quick clays" in Nordic countries (Geertsema, 2013). "Quick clays" are originally deposited in a salt-rich marine

680 environment in the Northern hemisphere during glaciation where they formed an electrostatically bonded double-layer structure including a cation (e.g. sodium) between two clay particles. When these clays become no longer subjected to salt water conditions (due to isostatic uplifts in Nordic countries, due to decrease of the Dead Sea level in our study area) and fresh water infiltrates these clays washing away the cations, the clay particles do not remain in a stable bonded structure and change to a liquid behaviour.

685 Such a process was previously proposed by Arkin and Gilat (2000) for the Dead Sea sinkholes, although the relatively low clay content of up to 20% detected in the fine material sediments around the Dead Sea (e.g. Khlaifat et al. 2010) indicates that such a process accounts for only a minor portion of the subrosion process.

690 In line with Krawczyk et al. (2015), we therefore propose a new, combined process model based on both chemical and mechanical erosion: the fine material stacks of marl, silt and clay within the alluvial fan change progressively from solid to liquid behaviour in the contact area of the fresh water inflow due to (chemical) leaching of the carbonate and evaporite particles first. Secondly, the clay particles are mechanically destabilized and eroded along the path of the subsurface water flow after loss of the (physical) stabilizing cations of the double layer structures. This process results in rapidly growing

695 subsurface channels and cavities in very short times, continuously amplified by the increasing (mechanical) kinetic energy of the water stream as documented for a spring by Al-Halbouni et al. (2017). Thirdly, even alluvial material at the subrosion interface gets washed out. The cavities extend horizontally and grow upward until the gravitation force of overlying alluvial stratum exceeds its bonding forces. This initializes a sudden sinkhole. The process is controlled by the long-term, seasonal and ephemeral

700 movement of the salt- fresh water interface (Salameh and El-Naser, 2000, Alrshdan, 2012), the volume of the fresh water flow and its velocity, the volume of buried soluble and/or mechanically erodible material and its mechanical properties within the alluvial fan.

7. Conclusions

The shear wave reflection seismic study at the Ghor Al-Haditha sinkhole investigation site was the first

705 experiment where this geophysical investigation method was applied in the environment of the Dead Sea. The achieved depth sections demonstrate that the technique can be applied in alluvial fan deposits in arid areas, which opens new feasibilities for shallow subsurface exploration of the Dead Sea sinkhole problem in high-resolution.

In general, the profiling results show a complex contact area between the high-energy prograding alluvial

710 fans of the Wadi Ibn Hammad and Wadi Mutayl and the low-energy lacustrine sedimentation environment of the Dead Sea. All available outcrop and borehole lithological data show no evidence for any thick massive salt layers in the shallow subsurface of the survey area down to 51 m depth below ground surface. This range can be extended with the new seismic data, which do not give any indication of a thick (> 2 m) compacted salt layer down to 200 m depth below the ground surface. Furthermore,

715 there are no structural indications of diapiric uplifts in the survey area. Also, since the hard rock basement was not detected down to that depth, the thickness of the Pliocene-Recent alluvial-lacustrine sequence is >200 m.

Based on the shear wave reflection seismic results, and supported by the drilled stratigraphy, our new model for the sinkhole process at the Ghor Al-Haditha sinkhole site suggests that the dissolution of small,

720 distributed inclusions of marl, silt, clay, and evaporites within the alluvial fan is enhanced by freshwater intrusions from the eastern wadis. Furthermore, we propose that such chemical erosion in the subsurface exists in a feedback with mechanical erosion of weak material, especially silt and clay, and with higher flow velocities of poorly consolidated alluvial material also. The process is not restricted to the depth of the "silt and clay" layer detected in the boreholes BH1 and BH2 and outlined in the area, it can also affect

725 shallower or deeper layer-like inclusions of weak, soluble, non-massive lacustrine material.

Consequently, geophysics-based mapping of areas prone to sinkhole hazard at the Dead Sea should consider different lithological controls on the location of sinkhole development.

Competing Interests: The authors declare that they have no conflict of interests.

8. Acknowledgements
730

The investigation was operated in the framework of the DEad SEa Research Venue (DESERVE), a virtual research institute of the Helmholtz Association, designed as a cross-disciplinary and cooperative international project of the Helmholtz Centres KIT, GFZ, UFZ, and their partners. The authors gratefully acknowledge the DESERVE Virtual Institute for continuous financial support of the investigations. The
735 geology group of the Jordan Ministry of Energy and Mineral Resources (MEMR) - formerly Natural Resource Authority (NRA) of Jordan – provided professional logistic support during equipment shipping and data acquisition, as well as by their excellent field camp infrastructure at Ghor Al-Haditha, enabling a fast access to the investigation area. Special thanks to Alexandra Carina Gassner, and Khalil Abu Ayyash for the support during the project. We are grateful to Damien Closson providing us a high-quality copy of
740 the El-Isa et al. (1995) report.

9. References

Abelson, M., Y. Yechieli, G. Baer, G. Lapid, N. Behar, R. Calvo, and M. Rosensaft: Natural versus human control on subsurface salt dissolution and development of thousands of sinkholes along the Dead Sea coast. Journal of Geophysical Research: Earth Surface, 122, 2017. DOI: 10.1002/2017JF004219.
745

Abelson, M., Yechieli, Y., Crouvi, O., Baer, G., Wachs, D., Bein, A. and Shtivelman, V.: Evolution of the Dead Sea sinkholes. In: Enzel, Y., , Agnon, A. & Stein, M., (Eds), New frontiers in Dead Sea paleoenvironmental research. Geological Society America Special paper, 401. P. 241-253, 2006, DOI: 10.1130/2006.2401(16).
750

Abelson, M., Gabay, R., Shalev, E., Yechieli, Y.: Sinkhole hazard around the evaporation ponts Dead Sea southern basin. Geological Survey of Israel, Report GSI/27/2009, 2009.

Abou Karaki, N, Fiaschi, S, and Closson, D.: Sustainable development and anthropogenic induced
755 geomorphic hazards in subsiding areas. Earth surf. Process. Landforms, 41, p. 2282-2295, 2016. DOI: 10.1002/esp.4047.

Abueladas, A., Al-Zoubi, A.: The application of a combined geophysical survey (GPR and seismic refraction) for mapping sinkholes in Ghor Al-Haditha Area, Jordan. Fall Meeting Supplement. EOS
760   Transactions, American Geophysical Union, 85, p. 47 (Abstract GP11A-0825), 2004.

Al-Halbouni, D., Holohan, E.P., Saberia, L., Alrshdan, H., Sawarieh, A., Closson, D., Waltera, T.R., Dahm, T.: Sinkholes, subsidence and subrosion on the eastern shore of the Dead Sea as revealed by a close-range photogrammetric survey. Geomorphology, 285, p. 305-324, DOI:
765   10.1016/j.geomorph.2017.02.006, 2017.

Alrshdan, H.: Geophysical Investigations of Ghor Haditha Sinkholes, Jordan. EAGE Workshop on Dead Sea Sinkholes – Causes, Effects and Solutions, Session 1: Geology, Hydrogeology & Hydrochemistry of Sinkholes, DOI: 10.3997/2214-4609.20143060, 2012.
770
Aki, K., Richards, P.G.: Quantitative seismology. W.H. Freeman and Company, San Francisco, 1980.

Arkin, Y., Gilat, A.: Dead Sea sinkholes—an ever-developing hazard. Environmental Geology 39 (7), p. 711–722, 2000.
775
Barjous, M., Sweidan, G., AL-Atteyat, N.: Geophysical and geological investigation of sinkholes in Ghor Al-Haditha area, Sinkhole project of Ghor Al-Haditha area (phase 4). Natural Resources Authority, Internal Report, Amman, 2004.

780   Batayneh, A., Abueladas, A., and Moumani, K.: Use of ground-penetrating radar for assessment of potential sinkhole conditions: an example from Ghor Al-Haditha area, Jordan. Environmental Geology 41, p. 977-983, 2002.

Bodet, L., Galibert, P.Y., Dhemaied, A., Camerlynck, C., Al-Zoubi, A.: Surface-wave profiling for
785   sinkhole hazard assessment along the eastern Dead Sea shoreline (Ghor Al-Haditha, Jordan). 72nd EAGE Conference & Exhibition incorporating SPE EUROPEC 2010, Barcelona, Spain, 14–17 June 2010 (M027), 2010.

Bookman (Ken-Tor), R., Enzel, Y., Agnon, A., Stein, M.: Late Holocene lake levels of the Dead Sea.
790   Geol. Soc. Am. Bull. 116, p. 555–571, 2004.

Camerlynck, C.M., Abueladas, A., Al-Ruzouq, R., Al-Zoubi, A., Boucher, M., Bodet, L., Dhemaied, A., and Galibert, P.Y.: Geophysical assessment of sinkhole hazard evaluation at Ghor Haditha (Dead sea, Jordan). Expanded Abstract DS07, EAGE Workshop on Dead Sea Sinkholes – Causes, Effects &
795   Solutions, 23.-26. September 2012, Amman, Jordan, 2012.

Closson, D.: Structural control of sinkholes and subsidence hazards along the Jordanian Dead Sea coast. Environmental Geology 47, p. 290–301, 2005.

800 Closson, D., Abu Karaki, N.: Salt karst and tectonics: sinkholes development along tension cracks between parallel strike-sleep faults, Dead Sea, Jordan. Earth Surface Processes and Landforms 34, 1408–1421. http://dx.doi.org/10.1002/esp.1829, 2009.

Crawford, J.M., Doty, W.., and Lee, M.R.: Continuous signal seismograph. Geophysics, 25, p. 95 – 105, 805 1960.

Dhemaied, A.: Tomographie seismique d'une zone de subsidence (Sinkhole zone, Ghor Al-Haditha, Jordanie). MSc Report (unpublished), Paris University, Paris, France, 2007.

810 Diabat, A.A.: Sinkholes related to Tectonic Factor at Ghor Al Haditha Area, Dead Sea, Jordan. Hydrogeologie und Umwelt, 33, p. 1-17, 2005.

Dix, C. H.: Seismic velocities from surface measurements: Geophysics, 20, p. 68–86, 1955.

815 El-Isa, Z.H., Rimawi, O., Jarrar, G., Abu-Karaki, N., Taqieddin, S.A., Atallah, M., Seif El-Din, N., Al-Saed, A.: Assessment of the hazard of subsidence and sinkholes in Ghor Al-Haditha area. Report submitted to Jordan Valley Authority. University of Jordan, Amman (141 pp.). University of Jordan, Center For Consultation, Technical Services and Studies, Amman, 1995.

820 Ezersky, M.: The seismic velocities of Dead Sea salt applied to the sinkhole problem. Journal of Applied Geophysics 58, p. 45–58, 2006.

Ezersky, M., Legchenko, A., Camerlynck, C., Al-Zoubi, A., Eppelbaum, L., Keydar, S., Baucher, M., Chalikakis, K.: The Dead Sea sinkhole hazard — new findings based on a multidisciplinary geophysical 825 study. Zeitschrift Für Geomorphologie N.F. 54 (2), p. 69–90, 2010. DOI:10.1127/0372-8854/2010/0054S2-0069.

Ezersky, M.G., Eppelbaum, L.V., Al-Zoubi, A., Keydar, S., Abueladas, A.-R., Akkawi, E., Medvedev, B.: Geophysical prediction and following development sinkholes in two Dead Sea areas, Israel and 830 Jordan. Journal of Environmental Earth Sciences, 70 (4), p. 1463-1478, 2013a. DOI: 10.1007/s12665-013-2233-2.

Ezersky, M., Bodet, L., Akkawi, E., Al-Zoubi, A., Camerlynck, C., Dhemaied, A., Galibert, P.-Y.: Seismic Surface-wave prospecting methods for sinkhole hazard assessment along the Dead Sea shoreline.

835   Journal of Environmental and Engineering Geophysics 18 (4), p. 233-253, 2013b. DOI:
        10.2013/JEEG18.4.233.

        Ezersky, M., Keydar, S., Al-Zoubi, A., Eppelbaum, E.: Sinkhole hazard assessment of the Dead Sea area
        in Israel and Jordan: A multidisciplinary study. Final Technical Report Project M27-050, US Agency for
840   International Development; Bureau of Global programs, Field Support and research; Center of Economic
        Growth and Agricultural Development, Washington D.C., 142p., 2013c.

        Ezersky, M., Frumkin, A.: Fault-Dissolution front relations and the Dead Sea sinkhole problem.
        Geomorphology 201, p. 35-44, 2013.
845

        Ezersky, M., Livne, E.: Geotechnical and geophysical properties of soils in the Dead Sea sinkhole
        problem. Near Surface Geoscience, Bochum, Germany, Expanded Abstract Mo P 13, 5p., 2013.

        Ezersky, M.G., Legchenko, A., Eppelbaum, L., Al-Zoubi, A.: Overview of the geophysical studies in the
850   Dead Sea costal area related to evaporate karst and recent sinkhole development. Int. Journal of
        Speleology 46(2), p. 227-302, 2017.

        Fiaschi, S., Closson, D., Abou Karaki, N., Pasquali, P., Riccardi, P., Floris, M.: The complex karst
        dynamics of the Lisan Peninsula revealed by 25 years of DInSAR observations. Dead Sea, Jordan. ISPRS
855   Journal of Photogrammetry and Remote Sensing, 130, p. 358-369, 2017. DOI:
        10.1016/j.isprsjprs.2017.06.008.

        Forbriger, T.: Inversion of shallow-seismic wavefields Part II: Inferring subsurface properties from
        wavefield transforms. Geophys. J. Int., Vol. 153, 735-752, 2003.
860

        Ford, D., Williams, P.: Karst Hydrogeology and Geomorphology. Wiley and sons, Chichester, 562 p.,
        2007.

        Frumkin, A., Ezersky, M., Al-Zoubi, A., Akkawi, E., Abueladas, A.-R.: The Dead Sea hazard:
865   geophysical assessment of salt dissolution and collapse. Geomorphology, 134, p. 102–117, 2011. DOI:
        10.1016/j.geomorph.2011.04.023.

        Frydman, S., Charrash, J., Goretsky, I.: Geotechnoical properties of evaporate soils of the Dead sea area.
        Engineering geology, 101, p. 236-244, 2008.
870

        Geertsema M.: Quick Clay. In: Bobrowsky P.T. (eds) Encyclopedia of Natural Hazards. Encyclopedia of
        Earth Sciences Series. Springer, Dordrecht, 2013.

875 Ghose, R., Brouwer, J., Nijhof, V.: A Portable S-wave vibrator for high-resolution imaging of the shallow subsurface. 59th EAGE Conference and Technical Exhibition, Amsterdam, The Netherlands, Expanded Abstracts MO37, 4 p., 1996.

Gilbert, G.K.: The topographic features of lake shores. US Geol. Surv. Ann. Rep., 5, p. 69–123, 1885.

880 Gorstein, M., and Ezersky, M.: Combination of HVSR and MASW methods to obtain shear wave velocity model of subsurface in Israel. IJGE 1(1), p. 20-41, 2015. DOI 10.15273/ijge.2015.01.004.

Inazaki, T.: High resolution reflection surveying at paved areas using S-wave type land streamer. Exploration Geophysics, 35, p. 1-6, 2004.

885

Keydar, S., Bodet, L., Camerlynck, C., Dhemaied, A., Galibert, P.-Y., Ezersky, M.G., Dror, O., Akkawi, E., Al-Zoubi, A.: A new approach for shallow subsurface imaging and its application to the Dead Sea sinkhole problem. 73th EAGE Conference and Technical Exhibition, Vienna, Austria, Expanded Abstracts A401, 4 p., 2011.

890

Khalil, B. M.: The geology of the Ar-Rabba area, map sheet No. 3152 IV. NRA, Mapping Project Bull., 22, 106p., 1992.

Khlaifat, A., Al-Khashman, O., Qutob, H.: Physical and chemical characterization of Dead Sea mud.
895 Materials Characterization 61, p. 564-568, 2010.

Krawczyk, C.M., Polom, U., Trabs, S. & Dahm, T.: Sinkholes in the city of Hamburg – New urban shear wave reflection seismic system enables high-resolution imaging of subrosion structures. Journal of Applied Geophysics, 78, p. 133-143, 2012. DOI: 10.1016/j.jappgeo.2011.02.003.

900

Krawczyk, C.M., Polom, U., Alrshdan, H., Al-Halbouni, D., Sawarieh, A. & Dahm, T.: New process model for the Dead Sea sinkholes at Ghor Al Haditha, Jordan, derived from shear-wave reflection seismics. Geophysical Research Abstracts, 17, EGU2015-5761, 2015.

905 Legchenko, A., Ezersky, M., Boucher, M., Camerlynck, C., Al-Zoubi, A., and Chalikakis, K.: Estimating sinkhole hazard in the Dead Sea costal area using P-wave velocities and magnetic resonance soundings. Near Surface 2008, Krakow, Poland, Expanded Abstract P18, 5p., 2008.

Park, C., Miller, R., and Xia, J.: Multichannel analysis of surface waves. Geophysics, 64, p.800-808,
910 1999.

Park, C.B., and Carnevale, M.: Optimum MASW survey - revisit after a decade of use: Geo-Institute Ann. Mtng (GeoFlorida 2010), February 20-24, 2010, West Palm Beach, FL, 2010.

915   Polom, U.: Elimination of source-generated noise from correlated vibroseis data (the 'ghost-sweep' problem). Geophysical Prospecting 45, p. 571-591, 1997.

Polom, U., Druivenga, G., Grossmann, E., Grüneberg, S., Rode, W.: Transportabler Scherwellenvibrator. Patent application DE 103 27 757 A1, Deutsches Patent- und Markenamt (in German), 2011.

920

Polom, U., Bagge, M., Wadas, S., Winsemann, J., Brandes, C., Binot, F., Krawczyk, C.M.: Surveying near-surface depotcentres by means of shear wave seismic. First Break, Vol. 31, p. 67-79, 2013.

Pugin, A.J.M., Larson, T.H ., Sargent, S.L.: Near-surface mapping using SH-wave and P-wave seismic
925   land-streamer data acquisition in Illinois, U.S. The Leading Edge 23, p. 677-682, 2004.

Pugin, A.J.M., Hunter, A.J., Motazedian, D., Brooks, G.R. and Kasgin, K.B.: An application of shear wave reflection landstreamer technology to soil response evaluation of earthquake shaking in an urban area, Ottawa, Ontario. Symposium on the Application of Geophysics to Engineering and Environmental
930   Problems (SAGEEP), Environmental and Engineering Geophysics society Annual Meeting, Denver, Colorado, U.S.A., April 1-5, 2007.

Pugin, A.J.M., Pullan, S.E., Hunter, J.A., and Oldenborger, G.A.: Hydrological prospecting using P- and S-wave landstreamer seismic reflection methods. Near Surface Geophysics, 7, p. 315-327, 2009.

935

Pugin, A.J.M., Pullan, S.E., Hunter, A.J.: Shear-wave high-resolution reflection in Ottawa and Quebec City, Canada. The Leading Edge, p. 250-255, 2013.

Rix, G.J. and Leipski, E.A.: Accuracy and resolution of surface wave inversion. In Bhatia, S.K., and
940   Blaney, G.W., eds., Recent Advances in Instrumentation, Data Acquisition and Testing in Soil Dynamics: Am. Soc. Civil Eng., p. 17–32, 1991.

Salameh, E., and El-Naser, H.: The interface configuration of the fresh-/Dead Sea water – Theory and measurements. Acta Hydrochimica Et Hydrobiologica, 28, No. 6, p. 323-328.

945

Sawarieh, A., Alrshdan, H.: The relation of sinkholes development in Ghor Al-Haditha area with the Dead Sea level fluctuations. Natural Resources Authority (Internal report), Amman, 2011.

Sawarieh, A., Abueladas, A.A., Al Bashish, M., and Al Seba'i, E.: Sinkholes Phenomena at Ghor Al-Haditha area: Sinkholes Project (Phase-2). Natural Resources Authority, Internal Report No.12, Amman., 2000.

Shalev, E., V. Lyakhovsky, and Y. Yechieli: Salt dissolution and sinkhole formation along the Dead Sea shore, J. Geophys. Res., 111, B03102, 2006. DOI: 10.1029/2005JB004038.

Taqieddin, S., Abderahman, N., Atallah, M.: Sinkhole hazard along the eastern Dead Sea shoreline area, Jordan: a geological and geotechnical consideration. Environmental Geology 39, p. 1237–1253, 2000.

Wachs, D., Yechieli, Y., Shtivelman, V.,Itamar, A., Bear, G., Goldman, M., Raz, E., Riebekov, M., and Shatner, U.: Formation of sinkholes along the shore of the Dead Sea - summary of finding from the first stage of research. Geological Survey Report GSI/41/2000 (in Hebrew), 49p., 2000.

Yechieli, Y., Wachs, D, Abelson, M., Crouvi, O., Shtivelman, V. Raz, E., Baer, G.: Formation of Sinkholes along the Shore of the Dead S – Summary of the first Stage of Investigation Geological Survey of Israel, Current Research, Vol. 13, p. 1-6, 2002.

Yechieli, Y., Abelson, M., Bein, M., Crouvi, O., Shtivelman, V.: Sinkhole "swarms" along the Dead Sea coast: reflection of disturbance of lake and adjacent groundwater systems. Geological Society of America Bulletin 118, p. 1075–1087, 2006. DOI: 10.1130/B25880.1.

Yilmaz, Ö.: Seismic Data Analysis. Society of Exploration Geophysicists, Tulsa, 2001.

Yilmaz, Ö.: Engineering seismology with applications to geotechnical engineering. In: Investigation in Geophysics Series No. 17, Ed. Richard D. Miller, Society of Exploration Geophysicists, Tulsa, 2015.

Figure Captions

Figure 1: (a) Generalized map of the Dead Sea area. Except the site Ghor Al-Haditha at the eastern border, which is the focus of this paper, the most sinkhole sites are located along the western shoreline of the Dead Sea (see e.g. Yechieli et al. 2002). (b) detailed map of the Ghor Al-Haditha sinkhole site and previous refraction seismic (El-Isa et al., 1995, Sawarieh et al., 2000) and MASW (Bodet et al., 2010) profiling. Boreholes BH1 and BH2 are reported in detail by El-Isa et al. (1995), two other boreholes are reported by Bodet et al. (2010) without any further information. Background is a Pleiades satellite image from 2015 combined with an aerial orthophoto mosaic from 2016.

985   **Figure 2**: Lithologic columns of the boreholes BH1 and BH2 from microscopic analyses, referenced to their surface elevation (black and white columns are originals of El-Isa et al. (1995)). The coloured, generalized columns are used for the figures of this paper. The main dip tendencies of the units toward the west are visible by the green connecting lines. The annotated borehole depths below the columns follow the written text in El-Isa et al. (1995).

990

Figure 3: Photos of the shear wave seismic reflection acquisition campaign carried out in October 2013. (a) Wheelbarrow-mounted shear wave source system on asphalt pavement at start location of profile 2. (b) Recording car, towed land streamer and source during operation on profile 3. (c) Land streamer towed by the recording car during acquisition on profile 2. Colour paintings on the road surface were used for
995   location numbering along the profiles. (d) Sledge-mounted horizontal geophone in SH (particle movement perpendicular to profiling direction) configuration along profile 3.

Figure 4: Map of the shear wave reflection seismic profiles acquired in 2013 (red lines) and 2014 (yellow lines). Green circles denote the locations of the boreholes made in 1994 (according to report of El-Isa et
1000   al. (1995)). Older refilled sinkholes are denoted by brown circles (after El-Isa et al. (1995)), blue circles (after Sawarieh et al. (2000)), and orange circle (after Bodet et al. (2010)). The dotted black polygon marks the main sinkhole and subsidence area after Al-Halbouni et al. (2017).

Figure 5: Examples of recorded shot gathers (AGC of 220 ms window, amplitude scaling and bandpass
1005   filter (18-20-78-82 Hz) applied) in time domain along profile 1b. The positions of the seismic source are labelled by orange stars. FFID denotes the record number along the profile, CHAN denotes the geophone number along the landstreamer unit. Arrows at top denote the condition of the ground surface observed along the profile. In the NE, close to the sinkhole affected area, first break and reflection signals are weak due to the strong wave scattering in the subsurface caused by material loosening and cracking. The
1010   situation improves towards SE, where no sinkholes or other subsidence features were present during profiling and the road surface was in good condition.

Figure 6: Examples of recorded shot gathers (AGC of 220 ms window, amplitude scaling and bandpass filter (18-20-78-82 Hz) applied) in time domain along profile 2b-2 (labelling as in **Fig. 5**). Good signal
1015   quality of first breaks and reflections mirrors a rather unaffected signal propagation in the subsurface, which correlates to the sinkhole-unaffected vicinity at surface. Reflection signals up to 400 ms in time represent layer responses from 70 m depth (applying 350 ms^{-1} shear wave propagation velocity).

Figure 7: Resulting depth section of profile 1b after post stack FD time migration (top) and interpretation
1020   of the main structure elements (bottom). Arrow bars at the top of the upper image denote the surface instability/stability as observed along the profile, while arrow bars below denote the road surface situation along the profile and the profile length. Black arrows at top indicate joints to crossing profiles. The lithology of borehole BH1 is projected from 10 m distance perpendicular into the profile. The interpreted

top of the "silt and clay" layer in BH1 is shown as the blue line along the profile, since it is the first layer detected at depth that is prone to subrosion. Also shown is the 1D shear wave velocity-depth function derived from seismic data in this area; this function was used for time-to-depth conversion of all profiles.

Figure 8: Resulting depth sections of combined profiles 2 and 2b-2 after post-stack FD time migration (top) and interpretation of the main structure elements (bottom). For annotations see **Fig. 7**. Lithology of boreholes BH1 and BH2 is projected perpendicular into the profile from 200 m distance, and therefore may not show the precise layering signature. Except the top 40 m the main characteristics down to 200 m show stacked sequences of NW-dipping reflectors, which are interpreted as NW-prograding alluvial fan sequences. The interpreted top of the "silt and clay" layer in BH1 and BH2 is shown by the blue line.

Figure 9: Combined depth sections of profiles 3 and 3b-2 after post stack FD time migration (top) and interpretation of the main structure elements (bottom). For annotations see **Fig. 7**. Lithology of boreholes BH1 and BH2 are projected from 400 m distance perpendicular into the profile, therefore probably not showing the precise layer signature. The interpreted top of the "silt and clay" layer in BH1 and BH2 is shown by the blue line. The centre part of the profiling track was repeatedly affected by recent sinkhole activity directly beside in the NE. For farming access it was refilled with gravel along more than 250 m, which was subsequently again affected by sinkholes and subsidence. This may cause the weaker reflection signatures in the upper 50 m if compared to profile 2 (**Fig. 8**). The main reflection pattern signature is similar to profile 2 and 2b-2, showing NW dipping events. In the SE of the profile a V-shaped structure is visible close to surface, filled with nearly horizontal reflection events, which is interpreted as a refilled channel side-cut. Due to the wide subsidence area NE of profile 3 the top of the "silt and clay" layer (blue line) was continued to NW starting from profile 1b instead using the projection of BH2.

Figure 10: Depth section of profile 4 after post stack FD time migration (top) and interpretation of the main structure elements (bottom). For annotations see **Fig. 7**. Lithology of boreholes BH1 and BH2 is projected from 200 m distance perpendicular into the profile. In contrast to profile 2, more gently NW-dipping events are present to 150 m depth, indicating less transportation energy of the alluvial material or an apparent structure dip. The top of the "silt and clay" layer in BH1 and BH2 is interpreted by the blue line. Bowl shaped signatures close to the surface in the SE indicate sinkhole-caused subsidence and/or refilled channel side-cuts. Significant reflection amplitudes of a stronger reflector pattern close to the NW end at nearly 90 m depth may indicate an evaporite-rich lense included in the alluvium-lacustrine deposits.

Figure 11: 3D representation of the 2.5D profiling grid (c.f., sections in **Fig. 7-10**, restricted to 200 m depth (no vertical exaggeration). Boreholes BH1 and BH2 are included as yellow bars representing the sand and gravel sequence above the detected „silt and clay" layer, the top of which is marked by a blue disc along each well shaft. Light blue lines along the profiles mark the interpreted continuation of the top of this layer starting from BH1 along profile 1 and subsequently continued to the crossing profiles. The

constructed horizon by triangular interpolation represents the derived top of the "silt and clay" layer
below the reference datum of -367 m a.s.l. based on the drilling and seismic results. At the deepest parts
1065   towards the Dead Sea border the top of this layer reaches nearly -467 m a.s.l., which is 60 m below the
level of the current alluvium/mud-flat transition of -407 m a.s.l. calculated by Al-Halbouni et al. (2017).